Spreading of thin volatile liquid droplets on uniformly heated surfaces

By VLADIMIR S. AJAEV

Department of Mathematics, Southern Methodist University, Dallas, TX 75275, USA

We develop a mathematical model for the spreading of a thin volatile liquid droplet on a uniformly heated surface. The model accounts for the effects of surface tension, evaporation, thermocapillarity, gravity and disjoining pressure for both perfectly wetting and partially wetting liquids. Previous studies of non-isothermal spreading did not include the effects of disjoining pressure and therefore had to address the difficult issue of imposing proper boundary conditions at the contact line where the droplet surface touches the heated substrate. We avoid this difficulty by taking advantage of the fact that dry areas on the heated solid surface are typically covered by a microscopic adsorbed film where the disjoining pressure suppresses evaporation. We use a lubrication-type approach to derive a single partial differential equation capable of describing both the time-dependent macroscopic shape of the droplet and the microscopic adsorbed film; the contact line is then defined as the transition region between the two. In the framework of this model we find that both evaporation and thermocapillary stresses act to prevent surface-tension-driven spreading. Apparent contact angle, defined by the maximum interfacial slope in the contact-line region, decays in time as a droplet evaporates, but the rate of decay is different from that predicted in earlier studies of evaporating droplets. We attribute the difference to nonlinear coupling between different physical effects contributing to the value of the contact angle; previous studies used a linear superposition of these effects. We also discuss comparison of our results with experimental data available in the literature.

1. Introduction

The evolution of a liquid droplet that spreads on a solid surface is known to depend on the local conditions near the contact line where the surface of the droplet touches the solid. Incorporating such local conditions into the standard description of viscous flow in the liquid results in a non-physical shear-stress singularity which can be removed by relaxing the no-slip condition for the viscous flow or introducing a microscopic precursor film (see Dussan V. 1979; de Gennes 1985 for reviews). Adding the effect of evaporation at the droplet surface may be expected to further complicate the problem and thus require some additional modelling assumptions. As we show below, this is not necessarily the case since evaporation alters the flow structure and thus allows us to employ mathematical models which are not appropriate for the isothermal case. The goal of this paper is to investigate moving contact lines in the presence of evaporation in the context of spreading and develop a mathematical model that does not involve any *ad hoc* assumptions about the value of the apparent contact angle. Developing such a model is especially important since moving contact lines in applications often appear when evaporation is also significant. Examples of

such applications include expanding and contracting vapour bubbles in actuators and micropumps (Oguz, Yuan & Prosperetti 1999), boiling in microchannels (Kandlikar 2002), as well as thin-film flows over heated surfaces (Kabov 2000; Gramlich *et al.* 2002).

Spreading can be analysed using a lubrication-type approach if droplet thickness is much smaller than its radius, as shown by Lopez, Miller & Ruckenstein (1976) and Greenspan (1978) for isothermal spreading. They took into account viscous and capillary effects and reduced the problem to a single partial differential equation for droplet thickness. A detailed investigation of the effect of different contact line models on droplet spreading was carried out by Haley & Miksis (1991). Additional physical effects, such as Marangoni stresses at the droplet surface and chemical reaction at the solid–liquid interface, were investigated later for non-volatile droplets in the framework of the same approach by Ehrhard & Davis (1991) and Braun *et al.* (1995). Experimental results for spreading of silicon oil on glass (Ehrhard 1993) are in agreement with the lubrication-type models.

The effect of evaporation in droplet spreading was considered by Anderson & Davis (1995) in the framework of the lubrication theory for a two-dimensional model. They used the one-sided model of evaporation which implies that all dynamical processes in the vapour are negligible. Corrections to the equilibrium value of the contact angle owing to contact-line motion and evaporation are both assumed relatively small and therefore their linear superposition is used to determine the contact angle. The dynamic contribution to the contact angle (owing to the flow near the moving contact line) is approximated by a linear relation between the speed and the cube of the contact-angle departure from the equilibrium value. Later, Hocking (1995) suggested that a different model for the dynamic contribution to the contact angle is more appropriate, but used the same superposition principle to investigate the combined effect of evaporation and fluid flow on the contact-line motion. Formulae for the corrections to the equilibrium value of the contact angle due to contact line motion in both papers are motivated by experiments with no evaporation at the droplet surface.

In the present work, we use a different approach to contact-line modelling suggested by Potash & Wayner (1972) and Moosman & Homsy (1980) in their studies of steady contact lines on heated surfaces. It relies on the description of dry areas on heated surfaces by microscopic adsorbed films which are in thermodynamic equilibrium with both solid and vapour phases. Such equilibrium can be achieved for non-zero film thickness owing to action of London–van der Waals forces. The pressure in the film due to these forces is inversely proportional to the cube of film thickness. We note that the adsorbed film is introduced here, not as an artificial tool needed to remove the singularity at the contact line, but rather as a physical effect with experimental verification (e.g. Bascom, Cottington & Singleterry 1964; DasGupta *et al.* 1993). The adsorbed film is always formed on the solid surface if the droplet is surrounded by vapour. A macroscopic interfacial shape, such as liquid film or constant-curvature meniscus, has to approach the adsorbed-film solution when the macroscopically dry region is approached. The contact line is then defined as the region of rapid change of interfacial curvature where the transition between the macroscopic shape and the adsorbed film takes place. The approach has been used successfully by DasGupta *et al.* (1993) and Morris (2001) for finding local solutions near the contact lines on heated surfaces and by Ajaev & Homsy (2001) for finding global shapes of steady vapour bubbles in microchannels. It has not been applied to spreading of volatile liquids on heated surfaces even though microscopic films are often used in models of isothermal spreading (de Gennes 1985; Glasner 2003).
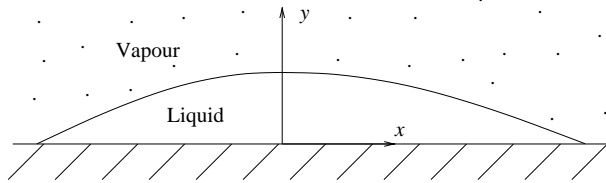
FIGURE 1. A sketch of a thin volatile liquid droplet spreading on a uniformly heated surface. Cartesian coordinates are shown.

This approach was originally developed for liquids which are perfectly wetting under isothermal conditions. One of the main challenges in modelling contact lines with evaporation is to generalize this approach to the case of partial wetting. The assumption that the disjoining pressure is an inverse power of the film thickness is no longer applicable for this case. Two different approaches can be taken. We can use an experimentally motivated disjoining pressure curve that accounts for both attractive and repulsive interactions; the contact angle is then related to the area under this curve (Churaev, Starov & Derjaguin 1982; Wong, Morris & Radke 1992). Generalization of this approach to the case with evaporation is straightforward (V. S. Ajaev & G. M. Homsy, unpublished work). Alternatively, we can derive a slope-dependent expression for the disjoining pressure near the contact line by integrating over all intermolecular interactions with a simple model potential and a cutoff length, following Miller & Ruckenstein (1974), Hocking (1993) and Wu & Wong (2004). The latter approach is taken in the present work. We believe that both approaches are capable of describing experimental results, but we do not attempt a detailed comparison here.

In the present work, we develop a model of spreading of a droplet of either perfectly or partially wetting volatile liquid on a uniformly heated surface. The droplet is in direct contact with a large reservoir of vapour. The model incorporates the effects of surface tension, gravity, evaporation, thermocapillarity and disjoining pressure in the framework of a lubrication-type approach. We note that many previous theoretical investigations of spreading have been carried out in the framework of two-dimensional models, while axisymmetric shapes are clearly more relevant experimentally. Therefore, we first present a complete formulation of the problem and discuss the several important results in the framework of a two-dimensional model to facilitate an easy comparison with the previous work. Then we proceed to the case of the axisymmetric spreading and discuss the comparison of our results with experiments.

2. Formulation

We consider a two-dimensional droplet of a volatile liquid of density ρ and viscosity μ on a uniformly heated rigid surface, as shown in figure 1. The fluid flow in the vapour phase directly above the liquid is, in general, coupled to the liquid flow in the droplet. However, in this study, we use the one-sided model of evaporation of Burelbach, Bankoff & Davis (1988). It implies that the density, dynamic viscosity and thermal conductivity of the vapour phase are very small compared to those of the liquid. Therefore, we take the limit when the corresponding non-dimensional ratios approach zero. However, the vapour density is retained in the boundary conditions where it multiplies the vapour velocity, which can be large.

We define the capillary number according to

$$C = \frac{\mu U}{\sigma_0}, \tag{1}$$

where σ_0 is the surface tension at the equilibrium saturation temperature, T_S^*, and the characteristic velocity is determined from the interfacial mass balance as

$$U = \frac{kT_S^*}{\rho \mathscr{L} R_0}. \tag{2}$$

Here, k is the thermal conductivity of the liquid, $\mathscr{L}$ is the latent heat of vaporization per unit mass, and R_0 is the initial radius of the droplet.

Let us consider the limit of small capillary numbers. In order to obtain physically meaningful solutions, we consider distinguished limits when physical quantities, as well as parameters of the problem, scale as certain powers of the capillary number. Solutions are obtained from the leading-order terms of an asymptotic expansion in powers of $C^{1/3}$. We note that it is often convenient to consider an asymptotic expansion in terms of an aspect ratio of the droplet. However, the cube of the aspect ratio has to scale as the capillary number in order for this approach to result in experimentally relevant solutions (Anderson & Davis 1995), so it is essentially equivalent to our asymptotic expansion in powers of $C^{1/3}$. For simplicity we carry out the derivation for a perfectly wetting liquid with disjoining pressure being inversely proportional to the cube of the thickness of the liquid layer on the solid surface. A more general case of the slope-dependent disjoining pressure is discussed briefly in the end of the next section.

Let us choose the length scales in the horizontal and vertical directions as R_0 and $C^{1/3}R_0$, respectively; the resulting non-dimensional Cartesian coordinate system, (x, y), is shown in figure 1. The vapour–liquid interface in our formulation is represented by a function $y = h(x, t)$, where t is the time variable scaled by R_0/U. We choose $C^{1/3}U$ as the velocity scale in the y-direction and $C^{1/3}\sigma_0/R_0$ as the pressure scale. The governing equations at leading order take the usual lubrication-type form:

$$-p_x + u_{yy} = 0, \tag{3}$$
$$-p_y - B = 0, \tag{4}$$
$$u_x + v_y = 0, \tag{5}$$
$$T_{yy} = 0. \tag{6}$$

Here, $B = \rho g R_0^2/\sigma_0$ is the Bond number, g is the acceleration due to gravity; the velocity in the x-direction is scaled by U, the non-dimensional temperature T is defined in terms of the dimensional one, T^*, according to

$$T = \frac{T^* - T_S^*}{C^{2/3} T_S^*}. \tag{7}$$

Let us now turn to the interfacial boundary conditions. In order to include the non-dimensional evaporative mass flux J into the leading-order mass-conservation condition, we scale the dimensional flux by $\rho U C^{1/3}$. With this choice and the above length and velocity scales, the non-dimensional leading-order conditions for conservation of mass and energy at the interface are written in the form:

$$J + uh_x - v = -h_t, \tag{8}$$
$$J = -T_y. \tag{9}$$

Equation (9) can be interpreted as the balance between the heat conducted through the droplet and the latent heat of the phase change at the interface. Heat transfer from the liquid film to the vapour is assumed negligible here, but it can be easily accounted for in the framework of our approach. The normal stress condition at the interface includes contributions from capillarity and disjoining pressure:

$$p - p_v = -h_{xx} - \frac{\varepsilon}{h^3}, \tag{10}$$

where p_v is the non-dimensional vapour pressure. We assume that the disjoining pressure is inversely proportional to the cube of film thickness and introduce a non-dimensional parameter, $\varepsilon = |A|/(\sigma_0 R_0^2 C)$, which is assumed to be an order of one quantity in the asymptotic limit $C \to 0$, although its numerical value may be small ($\sim 10^{-3}$); A is the Hamaker constant.

We assume that the surface tension is a linear function of temperature,

$$\sigma = \sigma_0 - \gamma(T^* - T_S^*), \tag{11}$$

and introduce the modified Marangoni number $M = \gamma T_S^*/\sigma_0$. We note that this parameter is sometimes referred to as the capillary number, but in our case it is essentially equivalent to the modified Marangoni number introduced by Gramlich *et al.* (2002) for thin-film flows over topographic features. With this choice, the shear stress condition at the interface is written as

$$u_y = -M(T_x + h_x T_y). \tag{12}$$

The scaled interfacial temperature T^i is related to the local mass flux and pressure jump at the interface through the non-equilibrium condition, which can be written in the following form (Ajaev & Homsy 2001):

$$KJ = \delta(p - p_v) + T^i, \tag{13}$$

where

$$K = \frac{\rho U \sqrt{2\pi \bar{R} T_S^*}}{2\rho_v \mathscr{L} C^{1/3}}, \qquad \delta = \frac{\sigma_0}{\mathscr{L} \rho R_0 C^{1/3}}. \tag{14}$$

Here, $\bar{R}$ is the gas constant per unit mass, ρ_v is the vapour density. According to (13), the departures of local temperature at the interface from the equilibrium value are characterized by two non-dimensional parameters, K and δ. The kinetic parameter, K, measures the relative importance of kinetic effects at the interface. The parameter δ characterizes the effect of changes in liquid pressure on the local phase-change temperature at the interface. Derivation of (13) is based on a simple linear relation between the mass flux and the vapour pressure. We note that alternative approaches have been suggested in the literature (Rose 2000), but we do not attempt to review them here.

At the solid–liquid interface, the liquid velocity is zero and the non-dimensional value of the temperature is fixed at $T = T_0 > 0$. The non-dimensional temperature T_0 is an important control parameter in experiments.

3. Evolution equation

Let us now solve the re-scaled system of governing equations and boundary conditions. First, we note that according to (4) the pressure p can be written as

$$p = -By + p_1, \tag{15}$$

where p_1 is a function of x only. The momentum equation (3) can be integrated twice to give the lubrication-type velocity profile in the form

$$u = \tfrac{1}{2}p_{1x}(y^2 - 2yh) + M(Jh)_x y. \tag{16}$$

We now substitute this velocity profile into the mass-conservation condition at the interface to obtain

$$h_t + J = \tfrac{1}{3}(h^3 p_{1x})_x - \tfrac{1}{2}M[h^2(Jh)_x]_x. \tag{17}$$

The scaled flux J is related to the interfacial temperature according to the non-equilibrium condition at the interface, equation (13). The interfacial temperature, T^i, can be expressed in terms of the given temperature of the solid surface since, according to the scaled heat-conduction equation, the temperature profile in the film is linear in y. This allows us to express J in terms of the scaled difference between the wall and saturation temperatures, T_0, according to

$$J = \frac{T_0 - \delta(h_{xx} + \varepsilon h^{-3})}{K + h}. \tag{18}$$

Substituting this formula together with the expression for pressure in the liquid from the normal-stress balance, (10), into (17), results in the differential equation for the film thickness:

$$h_t - \frac{\delta(h_{xx} + \varepsilon h^{-3}) - T_0}{K + h} + \tfrac{1}{3}[h^3(h_{xx} + \varepsilon h^{-3} - hB)_x]_x$$
$$+ \tfrac{1}{2}M\left[h^2\left(\frac{T_0 - \delta h_{xx} - \delta\varepsilon h^{-3}}{Kh^{-1} + 1}\right)_x\right]_x = 0. \tag{19}$$

Equation (19) is the key equation in our analysis. Once it is solved for the film thickness, $h(x, t)$, all other field variables are known.

Let us now specify the boundary conditions for (19). The heated surface is assumed infinite, but numerical integration can only be performed on a finite interval, $[0, L]$. The value $x = 0$ corresponds to the symmetry point near the top of the droplet (see figure 1), which implies

$$h_x(0) = 0, \tag{20}$$
$$h_{xxx}(0) = 0. \tag{21}$$

The choice of L and the boundary conditions at the right end-point of the interval require more discussion. The length L has to be sufficiently large so that the heated surface is macroscopically dry near $x = L$, which, in our approach, implies that it is covered by a microscopic adsorbed film there. The evaporation and London–van der Waals forces balance each other in this microscopic film, which is always stable for the case of positive disjoining pressure ($\varepsilon > 0$). Thickness of the equilibrium adsorbed film is found from the condition of zero mass flux in (18):

$$h_{af} = \left(\frac{\delta\varepsilon}{T_0}\right)^{1/3}. \tag{22}$$

Since the adsorbed film is flat, all derivatives of h with respect to x have to be zero there. This condition can be satisfied for steady contact lines when an ordinary differential equation for the local thickness is solved using a shooting method, as shown by DasGupta *et al.* (1993) and Morris (2001). However, the issue has not been addressed for unsteady contact lines when a partial differential equation for

the droplet thickness has to be solved with, at most, two boundary conditions in the adsorbed film, since it is a fourth-order equation in x with two symmetry conditions, (20)–(21). A remarkable feature of the numerical solution illustrated below is that only two boundary conditions are sufficient to make sure that the film is flat near $x = L$. We choose these conditions in the form:

$$h(L) = h_{af}, \quad h_x(L) = 0. \tag{23}$$

The value of $L = 2$ used in our simulations below turns out to be sufficiently large to ensure that the contact line stays inside the computational domain.

Equation (19) with the above boundary conditions is solved numerically using a finite-difference approach on the interval $[0, 2]$ with 800 mesh points. The BDF method from the standard *DVODE* solver developed by Brown, Byrne & Hindmarsh (1989) is used to describe evolution in time numerically. Special care is needed in discretization of nonlinear terms as discussed by Zhornitskaya & Bertozzi (2000).

The above formulation can be used for partially wetting liquids as well, except that a slope-dependent expression for the disjoining pressure has to be employed in the normal stress balance at the interface. Following Wu & Wong (2004), we write the modified expression for Π in the form

$$\Pi = \frac{\hat{\varepsilon}}{h^3} \left[\alpha^4 + 2 h h_x^2 h_{xx} - h_x^4 \right], \tag{24}$$

where the constants $\hat{\varepsilon}$ and α are related to the strength of intermolecular interactions and thus the wetting properties of the liquid on a given substrate. We note that the expression for the equilibrium adsorbed film thickness, (22), can still be used for the case of the slope-dependent disjoining pressure if ε is replaced with $\hat{\varepsilon}\alpha^4$. Derivation of (24) relies on ideas from the earlier works of Miller & Ruckenstein (1974) and Hocking (1993) and involves summation of intermolecular interactions modelled by the van der Waals potential with a cutoff length. Equation (24) is valid only when the system is close to thermodynamic equilibrium. We assume that departures from thermodynamic equilibrium owing to phase change and contact line motion in our system are not large enough to alter the expression for the disjoining pressure significantly.

4. Quasi-steady evolution of a two-dimensional droplet

Numerical solutions of (19) over a range of parameter values and initial conditions show rapid change of the interface shape followed by relatively slow evolution, which eventually leads to the complete disappearance of the droplet owing to evaporation. In this section, we investigate the latter regime, which we refer to as 'quasi-steady'. Droplet evolution in this quasi-steady regime is essentially independent from the initial conditions.

4.1. *Perfectly wetting liquid*

Let us first consider a liquid which is perfectly wetting under the isothermal conditions and assume that the Marangoni effect and gravity are negligible ($M = B = 0$). Estimates of the capillary number show that it is below 10^{-3} under typical experimental conditions, so our asymptotic approach is justified. Let us choose representative values of parameters $\bar{K} = 0.2$, $\delta = 10^{-3}$, $\varepsilon = 10^{-6}$. The disjoining-pressure parameter ε is difficult to measure experimentally, so its actual value may be different from 10^{-6}. However, our simulations show that the macroscopic shape of the interface is not very sensitive to the variations of ε as long as it is below 10^{-4}.
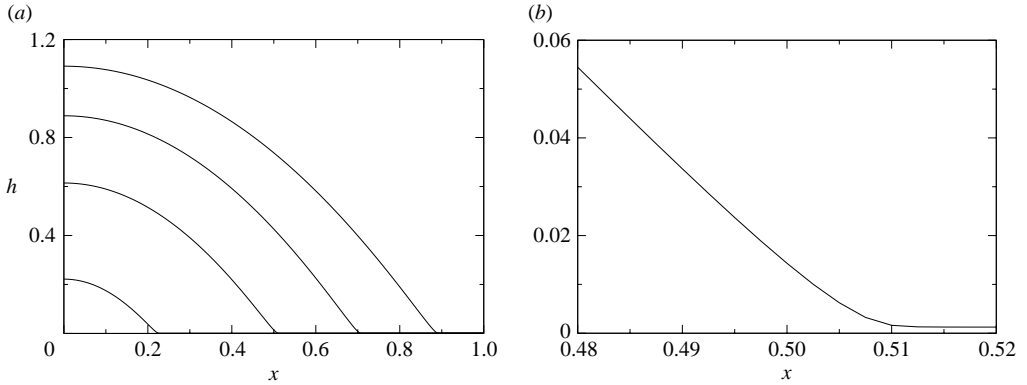
(*a*)

(*b*)

FIGURE 2. Shapes of evaporating droplet shown for four different values of $t(0.2, 0.6, 1.0, 1.4)$ for $T_0 = 0.5$ in the quasi-steady regime (*a*) and the blow-up of the contact-line region (*b*) showing the rapid change of curvature and matching onto the adsorbed film. The liquid is perfectly wetting under the isothermal conditions. The parameter values are chosen as $K = 0.2$, $\varepsilon = 10^{-6}$, $\delta = 10^{-3}$, $B = M = 0$.

We note that the small values of ε and δ may seem to impose severe limitations on the application of the asymptotic expansion in powers of $C^{1/3}$ since the higher-order terms in that expansion, e.g. $O(C^{2/3})$ corrections to the film thickness, can be larger in the absolute value than ε even for very small capillary numbers. However, the disjoining pressure becomes important only for very small values of thickness in the contact-line region. A local analysis of the double asymptotic expansion in $C^{1/3}$ and $\varepsilon^{1/2}$ in this region with an additional assumption that $\delta \sim \varepsilon^{1/2}$ shows that the leading-order behaviour of the solution is determined by $O(C^{1/3}\varepsilon^{1/2})$ terms which vary in space on a much faster scale than the contributions from $O(C^{2/3})$. Thus, our approach is expected to be applicable for the moderately small capillary numbers encountered in experiments.

Let us now discuss the choice of the initial conditions for solving (19) numerically. A constant-curvature droplet placed on top of a uniform adsorbed film may seem to be the most convenient choice, but this profile is not smooth and therefore results in non-physical rapid changes in the interface shape near the contact line at the initial stages of evolution. In order to reduce the effect of such variations on the solutions obtained in this section, we use the following procedure. First, we run the code with an artificial starting vapour–liquid interface profile given by the formula:

$$h_0(x) = \begin{cases} b - \dfrac{x^2}{b} & (x^2 < b(b - h_{af})), \\ h_{af} & (x^2 > b(b - h_{af})), \end{cases} \tag{25}$$

where $b = 1.2$. Once the droplet radius, defined by the maximum of the interfacial curvature as discussed below, decreases to the value of $a = 1$, the simulation is stopped. The profile recorded at this point is then used as the initial condition (i.e. the interface profile at $t = 0$) in all simulations discussed in this section.

A typical quasi-steady solution for the liquid which is perfectly wetting under the isothermal conditions is shown in figure 2(*a*). Snapshots of the interface are shown at equal time intervals, starting at $t = 0.2$, for $T_0 = 0.5$. The macroscopic part of the droplet has an almost uniform negative curvature and decreases its volume owing to evaporation. Since we are considering the limit of small C, i.e. strong surface
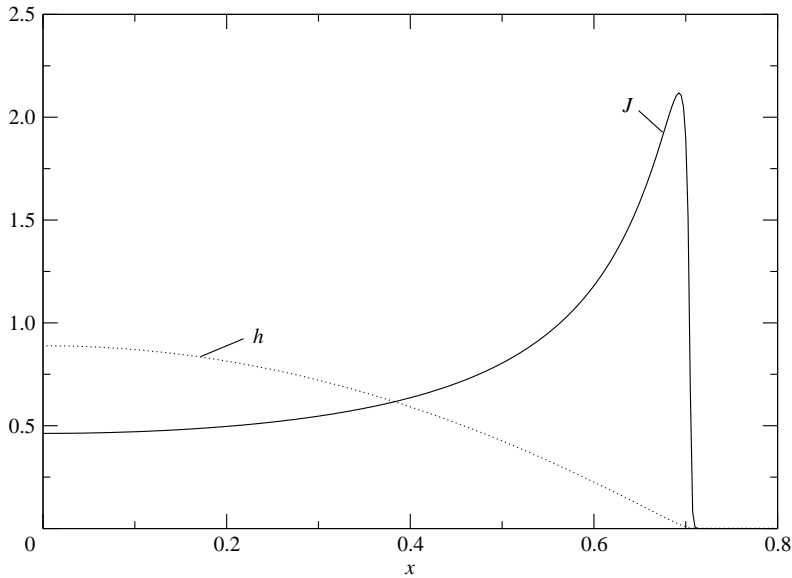
FIGURE 3. Typical evaporative flux profile along the interface (solid line) in the quasi-steady regime for $K = 0.2$, $\varepsilon = 10^{-6}$, $\delta = 10^{-3}$, $B = M = 0$, $t = 0.6$. The corresponding interface shape is shown by the dotted line.

tension, small variations of the curvature are sufficient to drive the flow towards the contact line. The contact line is represented by a localized region of rapid change of curvature moving from the right to the left in a manner similar to a slowly decaying solitary wave. The enlarged view of the contact line region is shown in figure 2(*b*). The curvature is positive and has a sharp maximum in this region. Transition between the macroscopic part of the interface and the flat adsorbed film is also clearly seen in figure 2(*b*); the film stays flat all the way to the right-hand end of the computational domain. We note that our representation of the contact-line region is somewhat analogous to interface representation in the phase-field method for numerical simulations of interfaces.

Let us now investigate the changes in the evaporative mass flux along the vapour–liquid interface. Figure 3 shows the flux profile at $t = 0.6$ together with the corresponding interface profile (dotted line). Clearly, the flux becomes larger as the contact line is approached since the film thickness and thus the denominator of the expression for J, (18), becomes smaller. The flux reaches a maximum near the contact line and then decays sharply owing to the effect of the London–van der Waals forces. We note that the mass-flux profile in the quasi-steady regime is similar to the steady-state results of Potash & Wayner (1972) and Moosman & Homsy (1980).

Several methods can be used to define the position of the contact line from our solution. We define it as the value of x that corresponds to the maximum of the interfacial curvature. This value, $a = a(t)$, is shown as a function of time for the quasi-steady regime in figure 4(*a*). Even though the droplet is two-dimensional, we often refer to a as the radius, following Anderson & Davis (1995). Clearly, a slow, approximately linear, decay in the radius for relatively large droplets is followed by a much faster change for smaller droplets. In order to explain these dynamics, we observe that the overall evaporation rate and thus the rate of change of volume remain almost constant when the droplet size changes in time. Thus, the radius,
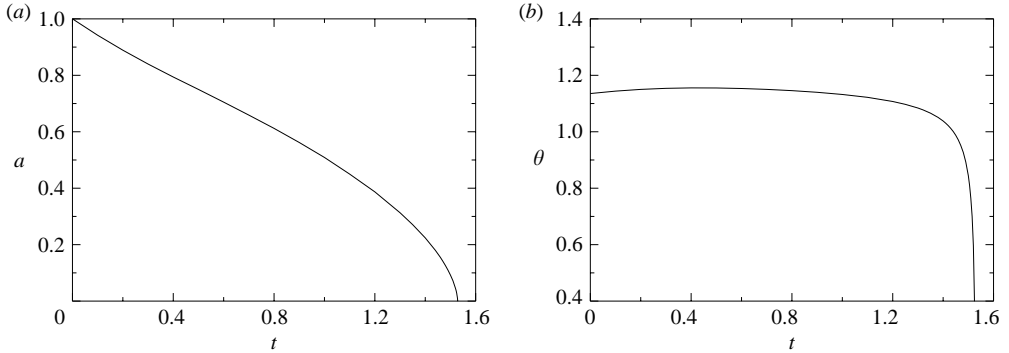
FIGURE 4. (*a*) The droplet radius defined by the maximum of curvature and (*b*) the apparent contact angle as functions of time for the quasi-steady evaporation of a volatile droplet for the same parameter values as in the previous two figures.

which scales as the square root of volume, has to decrease faster for smaller droplets. We have verified this explanation by re-plotting the data from figure 4(*a*) in log–log coordinates.

The maximum value of the interfacial slope, attained near the contact line, is used to define the apparent contact angle, θ, plotted in figure 4(*b*) as a function of time. The contact angle is almost constant for larger droplets and then decays rapidly for smaller droplets. We note that the contact angle seen in these simulations is sensitive to the local temperature. If the superheat is decreased to zero, the contact angle also approaches zero since our simplified expression for the disjoining pressure implies that the liquid is perfectly wetting under the isothermal conditions. Thus, the finite contact angle seen in figure 4(*b*) results from a balance between evaporation and disjoining pressure as opposed to a balance between different components of the disjoining pressure (e.g. in Glasner & Witelski 2003; Glasner 2003).

4.2. *Partially wetting liquid*

Let us now consider the quasi-steady regime for a droplet of a partially wetting liquid. We choose the same parameter values and initial conditions as in figure 4 except that we use the expression for the disjoining pressure given by (24) with $\hat{\varepsilon} = 10^{-4}$, $\alpha^4 = 10^{-2}$. We note that, in our approach, the contact angle is not zero even though the microscopic film is present; this situation is sometimes referred to as the case of 'pseudopartial wetting'. Droplet radius, $a = a(t)$, from this simulation is shown in figure 5(*a*), where the results for the perfectly wetting liquid are also included for comparison. The droplet radius initially decays rapidly to values smaller than the corresponding values in the previous subsection to accommodate the different value of the contact angle. However, over longer periods of time, it decays more slowly for a partially wetting liquid since a droplet of the same radius is larger and more difficult to evaporate in this case.

Figure 5(*b*) illustrates the apparent contact angle as a function of time for liquids with different wetting properties. The initial rapid change of the contact angle for the partially wetting case is due to the choice of initial conditions. We note that θ is the scaled quantity, so the actual value of the contact angle is still small even when θ is close to 1. The contact angle is clearly larger for the case of partial wetting, which supports the suggestion of Anderson & Davis (1995) that superposition of different physical effects contributes to the total value of the contact angle. However,
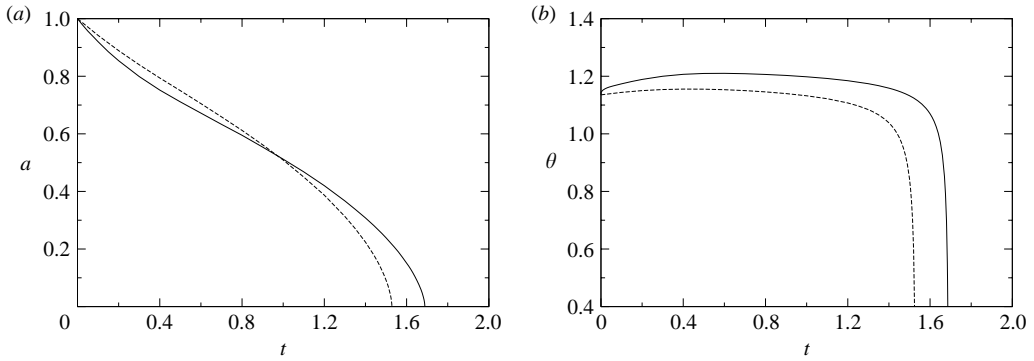
FIGURE 5. Typical plots of (a) the droplet radius and (b) the values of the apparent contact angle as functions of time for a partially wetting liquid ($\hat{\varepsilon} = 10^{-4}$, $\alpha^4 = 10^{-2}$, solid lines) in the quasi-steady regime. Solutions for the case of perfect wetting are also shown for comparison (dashed lines). For both cases $K = 0.2$, $T_0 = 0.5$, $\delta = 10^{-3}$.
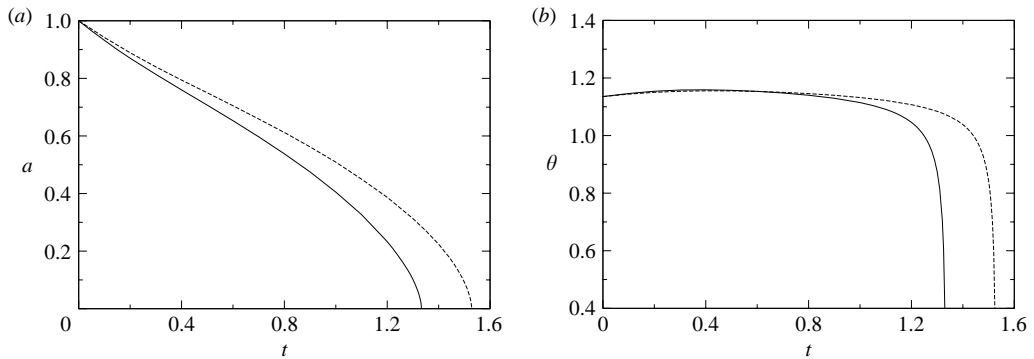

FIGURE 6. The effect of thermocapillary stresses on the droplet spreading. (a) The radius and (b) the contact angle are plotted as functions of time for $M = 1$ (solid lines) and $M = 0$ (dashed lines).

we must be cautious in making direct comparisons with previous work on partially wetting liquids since changing the value of α is not equivalent to changing the wetting properties of the liquid. Different contact angles under isothermal conditions correspond to different strengths of intermolecular interactions on microscale, so both α and $\hat{\varepsilon}$ have to be changed in a self-consistent fashion to describe a change in the wetting properties. Alternatively, we can investigate the dynamics of the apparent contact angle for fixed α and $\hat{\varepsilon}$. This latter approach is taken in the present work. The results in figure 5(b) indicate the same type of contact angle decay with time as was found by Anderson & Davis (1995), but the characteristic decay time is smaller. Thus, the nonlinear interactions between various physical effects in the vicinity of the contact line lead to smoothing of the sharp decay of the contact angle found from linearized models.

4.3. *The Marangoni effect*

Let us now discuss the effects of thermocapillary stresses, characterized by the modified Marangoni number, M, in the quasi-steady regime. Figure 6 illustrates the results obtained by solving (19) with $M = 1$ and the same values of other parameters as in figure 4. Droplet radius, shown in figure 6(a) as a function of time, is found to

decrease faster when the Marangoni effect is taken into account. This has a simple physical explanation. Since thermocapillary stresses act in the direction from the hotter regions near the contact line to the colder regions near the top of the droplet, they effectively slow down spreading. This effect also accounts for a slightly higher value of the apparent contact angle seen in figure 6(*b*) at the later stages of droplet evolution. The initial slight decrease in the contact angle is due to the somewhat artificial initial conditions. It is clear that the influence of thermocapillary stresses on the interface evolution in the quasi-steady regime is not large, especially since the value of the modified Marangoni number under typical experimental conditions is much less than $M = 1$ used in figure 6. This justifies the assumption of $M = 0$ used in many simulations in the present work.

Evolution of the droplet in the quasi-steady regime is characterized by simple features, such as monotonic decay of the drop radius due to evaporation. More complicated dynamics can be observed when evolution is highly unsteady. Let us now turn to this case.

5. Unsteady spreading of a two-dimensional droplet

The analysis of the quasi-steady regime in the previous section allows us to predict the values of the apparent contact angle on a heated surface of a given temperature for a droplet of a given size and material properties. These values turn out to be the same for a variety of different initial conditions as long as the quasi-steady regime is established. Thus, they are somewhat analogous to the equilibrium values of the contact angle without evaporation; we refer to them as quasi-equilibrium values. When the contact angle reaches the quasi-equilibrium value corresponding to the current droplet size, further evolution can be described as the slow disappearance of the droplet due to evaporation. In experiments, the interface shapes are often different from the quasi-equilibrium value, e.g. when the droplet is placed on the surface and starts spreading (Bourgés-Monnier & Shanahan 1995). Even though this rapid spreading is often outside the domain of applicability of the lubrication theory, we can simulate it in the framework of our model by choosing the initial value of the contact angle which is small, but significantly different from the quasi-equilibrium value. The purpose of such study is to understand the effects of evaporation on the capillary-driven spreading.

Let us consider the spreading of a perfectly wetting liquid characterized by the same parameter values as in the previous section for a range of values of the superheat. The initial conditions on the interval $[0, L]$ are in the form

$$h_0(x) = \begin{cases} 2(1 - x^2) + h_{af} & (x < 1), \\ h_{af} & (x > 1). \end{cases} \tag{26}$$

We note that the initial contact angle is larger than the quasi-equilibrium value for all relevant values of the superheat and therefore the droplet can be expected to spread on the heated surface owing to capillary forces. However, evaporation tends to prevent spreading; thus, there is a competition between evaporation and the tendency to spread owing to a mismatch in the contact angle. This is illustrated in figure 7(*a*) where droplet radius is shown as a function of time for two different values of the scaled superheat, $T_0 = 1$ and 0.2. Clearly, the droplet initially tends to spread on a relatively fast time scale, but then evaporation takes over and the radius decays monotonically on a much slower time scale corresponding to quasi-steady evolution.
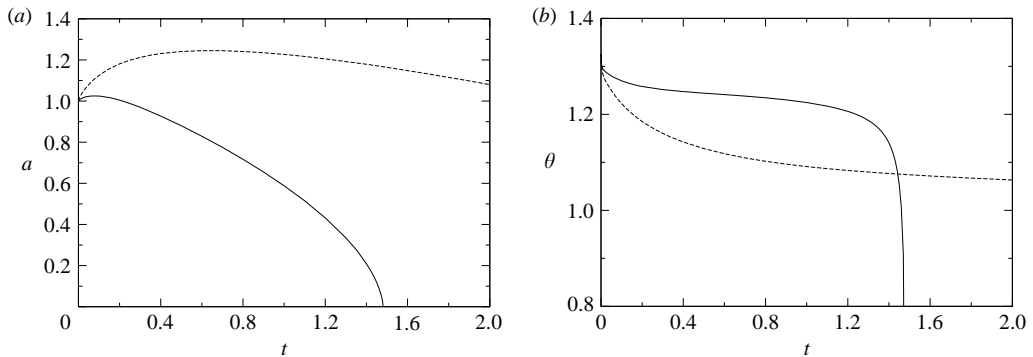
FIGURE 7. Competition between spreading and evaporation is illustrated by plots of (*a*) the radius and (*b*) the apparent contact angle as functions of time for two different values of the superheat: $T_0 = 1.0$ (solid lines) and $T_0 = 0.2$ (dashed lines).

For small T_0, evaporation does not have a significant effect on the initial spreading rate. For values of T_0 near or above 1, the quasi-steady regime is established almost immediately, as can be seen in figure 7(*a*), so spreading is effectively prevented owing to evaporation.

The apparent contact angle, defined as the maximum slope of the interface, is plotted as a function of time in figure 7(*b*) for the same two values of the scaled superheat as in figure 7(*a*). The contact angle changes rapidly in the beginning, but then decays almost linearly over a wide range of values of *t*. At the final stages of evaporation, the contact angle changes rapidly in the same fashion as described in the previous section. For small values of the superheat, such as $T_0 = 0.2$ in figure 7(*b*), the nearly linear decay is the dominating feature of the contact angle evolution over a significant period of time. We note that our results on unsteady spreading are similar to those of Anderson & Davis (1995) except that the changes of the contact angle on the fast time scale are not as rapid as predicted by their model. Based on the discussion of contact angle dynamics in §4, we can again attribute this to a nonlinear coupling between different factors contributing to the value of the contact angle.

In order to relate our results to previous studies of spreading under isothermal conditions, let us consider the limit of weak evaporation by decreasing the value of the non-dimensional superheat to $T_0 = 0.01$. Evolution of the droplet in this regime is dominated by spreading rather than evaporative mass loss. Thus, we expect results similar to the isothermal case. It is well known that, in isothermal spreading, the increase of the droplet radius with time can often be approximated by power laws in the form $a(t) \sim t^\beta$, where β is referred to as the spreading exponent (Greenspan 1978; de Gennes 1985). In particular, for pure capillary spreading without gravity, $\beta = 1/7$. Approximately the same dynamics are recovered in our simulations for the weak evaporation limit, as illustrated in figure 8(*a*). We plot radius versus time using log–log coordinates. The dashed line has the slope of 1/7. The slope of the solid line is slightly different from 1/7 since the effects of evaporation are not competely eliminated, but the agreement is clearly very good.

Let us now discuss the contact angle dynamics in the limit of weak evaporation. Typical results for the advancing contact angle as a function of local contact line speed during spreading are recorded in figure 8(*b*). The angle is increasing with *V* and the $\theta(V)$ curve is concave down, in agreement with numerous investigations of similar curves for the isothermal case (discussed e.g. in Eggers & Stone 2004). We
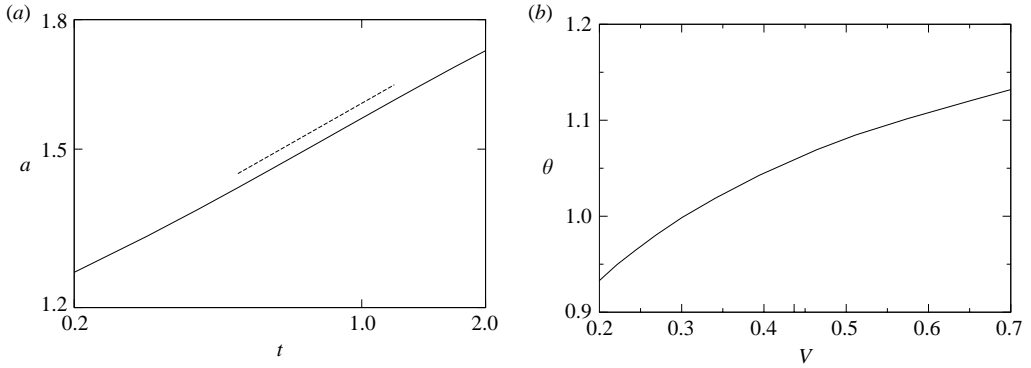
(a)

(b)

FIGURE 8. (a) Spreading dynamics and (b) contact angle versus velocity in the limit of weak evaporation, $T_0 = 0.01$.

also note that, in the weak evaporation limit, the approach of Anderson & Davis (1995) gives accurate predictions of the contact angle.

6. Evolution of an axisymmetric droplet

The above derivation of (19) has been carried out for the two-dimensional droplet in order to illustrate our lubrication-type approach and to facilitate comparison with previous work. However, in order to obtain experimentally relevant predictions, we have to consider axisymmetric spreading. We omit the derivation of the axisymmetric version of (19) since it follows the same steps as in the two-dimensional case discussed in §3. The final result is written in the form:

$$
h_t - \frac{\delta\left[h_{rr} + r^{-1}h_r + \Pi(h)\right] - T_0}{K + h} + (3r)^{-1}\left[rh^3(h_{rr} + r^{-1}h_r + \Pi(h) - hB)_r\right]_r
$$
$$
+ \frac{M}{2r}\left[rh^2\left(\frac{T_0 - \delta h_{rr} - \delta r^{-1}h_r - \delta\Pi(h)}{Kh^{-1} + 1}\right)_r\right]_r = 0. \quad (27)
$$

Here, r is the radial coordinate; the disjoining pressure, $\Pi(h)$, is in general capable of describing liquids with different wetting properties (Wu & Wong 2004), but in the simulations below is taken to be inversely proportional to the cube of the film thickness.

The boundary conditions for (27) are the two symmetry conditions at $r = 0$, the fixed adsorbed film thickness at $r = L$, and the condition of zero radial derivative at $r = L$. Numerical simulations of the system are carried out using the finite-difference method with time-stepping performed by the *DVODE* package (Brown *et al.* 1989). The derivatives of h with respect to r at the point $r = 0$ are evaluated analytically by considering small non-zero values of r and then taking the limit of $r \to 0$.

Numerical solution of (27) shows a moving localized region of rapid change of interfacial slope similar to the one illustrated in figure 2 for the two-dimensional case. The time-dependent position of this region, defined by the maximum of the interfacial curvature, is shown in figure 9(a). We use the same parameter values as in figure 4. The decay of the droplet radius is qualitatively similar to the two-dimensional case shown in figure 4(a). The apparent contact angle is defined by the maximum of the slope of the interface and plotted in figure 9(b). Initial slight increase in the contact angle seen in the figure is due to transient effects; the angle decays monotonically
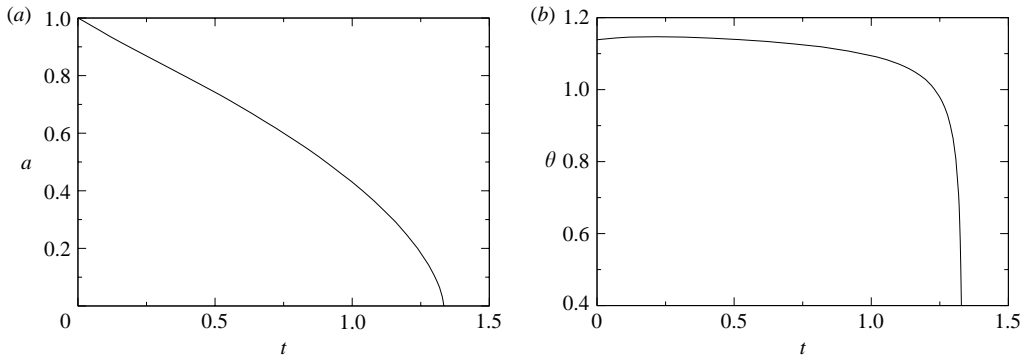
FIGURE 9. Evolution of an axisymmetric droplet of a perfectly wetting liquid for the quasi-steady regime for $K = 0.2$, $T_0 = 0.5$, $\varepsilon = 10^{-6}$, $\delta = 10^{-3}$, $M = B = 0$. (a) Droplet radius and (b) the apparent contact angle are shown as functions of time.

after the quasi-steady regime is established. Despite clear similarities between the two-dimensional and axisymmetric results, there are also quantitative differences. In particular, the rate of change of droplet radius is larger in the axisymmetric case, so that the droplet disappears faster than predicted by two-dimensional models. Thus, we have to be cautious about using two-dimensional models for comparison with experiments.

Let us discuss comparison of our axisymmetric results with some recent experimental data. Bourgés-Monnier & Shanahan (1995) have studied thin droplets of water and n-decane on different surfaces in the presence of evaporation. They measured droplet radius and contact angle as functions of time. We cannot expect a direct quantitative comparison of our results with their work, since in experiments there was no external heating. However, qualitative agreement can be expected, since the temperature gradient in the film is still present owing to local cooling of the surface owing to evaporation. We note that typical results for thin droplets in the quasi-steady regime, e.g. stages III′ and IV in figure 4 in Bourgés-Monnier & Shanahan (1995), show that the contact angle changes by a small amount (typically less than 10% of the original value) over a period of time of $t \approx 25$ min and then rapidly decays during a much shorter time ($t \approx 10$ min). This is consistent with the result shown in figure 9. We note that this also supports our conclusion about the nonlinear smoothing of the sharp decay in the contact angle found by Anderson & Davis (1995).

Gokhale, Plawsky & Wayner (2003) studied evaporation and condensation of droplets of n-butanol formed within a quartz cuvette that is partially filled with liquid and can be heated from either the top or the bottom. They carried out measurements of the radius of curvature of the droplet as a function of time in the regime when the droplet size slowly decreases owing to evaporation. Let us discuss the predictions of radius of curvature given by our model with values of non-dimensional parameters corresponding to n-butanol ($\rho = 810 \, \text{kg m}^{-3}$, $\mathscr{L} = 591.3 \, \text{kJ kg}^{-1}$, $k = 140 \, \text{W m}^{-1} \, \text{K}^{-1}$, $\mu = 3.3 \times 10^{-3} \, \text{Pa s}$, $\sigma_0 = 0.02 \, \text{N m}^{-1}$), the initial droplet radius of $20 \, \mu\text{m}$, and dimensional superheat $\Delta T^* = 0.01$ K. Results for scaled radius of curvature at the centre of the droplet, R^*, versus time obtained by solving (27) numerically are shown in figure 10. The droplet initially spreads, but then evaporation takes over and the radius of curvature decays at a rate of approximately $1 \, \text{mm s}^{-1}$.

We note that the actual values of wall superheat have not been measured experimentally. They are estimated to be of the order of 10^{-4}. The scalings of our asymptotic model are difficult to justify for such extremely small superheat, so
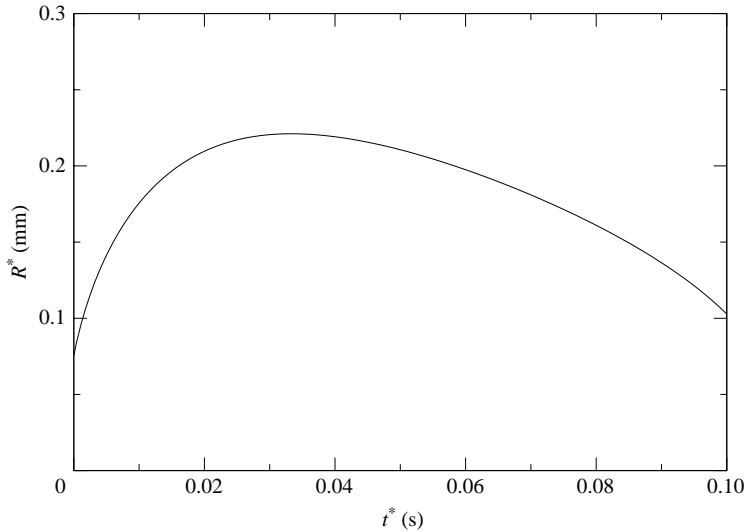
FIGURE 10. Droplet radius of curvature as a function of time for droplets of *n*-butanol
of initial radius of 20 μm found from the numerical solution of (27).

we will not attempt to present a direct comparison between theory and experiment.
However, we note that since dR^*/dt^* decreases approximately linearly with the
superheat, the value of rate of change of curvature for $\Delta T^* = 10^{-4}$ is expected to
be of the order of 10^{-2} mm s^{-1}, which is in reasonable agreement with the actual
experimental results of Gokhale *et al.* (2003). Experimental studies of droplets in
the range of superheats between 0.01 and 0.1 K with simultaneous measurements of
heated surface temperature are required to verify all aspects of the proposed model.

7. Conclusions

We have developed a mathematical model for the spreading of a thin volatile
droplet on a heated surface. The droplet is surrounded by vapour so that the heated
surface is covered with a microscopic adsorbed film of vapour. We use a lubrication-
type approach to derive an evolution equation for the droplet thickness. This equation
is capable of decribing not only the macroscopic droplet shape, which was studied
by previous investigators, but also the microscopic adsorbed film and the transition
region between the two. The contact line is then defined as the region of rapid change
of curvature in the numerical solution of this evolution equation. Thus, difficulties
in imposing appropriate boundary conditions at the contact line encountered in the
previous studies are avoided. This is somewhat analogous to the idea of avoiding
difficulties in describing sharp interfaces by using phase-field methods in numerical
simulations of moving interfaces.

The definition of the contact line as the transition region between the adsorbed film
and the macroscopic film or meniscus relies on the earlier works of Potash & Wayner
(1972) and Moosman & Homsy (1980). However, in these and many subsequent
investigations, the liquid is perfectly wetting and the contact line is either steady or
oscillating around a steady state. In the present work, the approach has been extended
in two new directions: describing unsteady motion of contact lines in the presence of
evaporation and modifying the theory to include the case of partially wetting liquids.
For the latter, we use a generalized formula for the disjoining pressure obtained by
integration of intermolecular interactions in the vicinity of the contact line.

The proposed model describes coupled effects of capillarity, Marangoni stresses, evaporation, gravity and disjoining pressure. The results indicate that the droplet dynamics is governed mostly by competition between evaporation and capillary spreading. We identify two regimes depending on the value of the superheat at the heated surface. For small values of the superheat the droplet is spreading on the surface in a fashion similar to the isothermal case. However, for large superheat, evaporation prevents spreading and the system quickly approaches the so-called quasi-steady regime characterized by slow evaporation and relatively weak fluid flow.

The results of our simulations have been compared with the previous theoretical work of Anderson & Davis (1995). We found that evolution of the droplet radius and contact angle is qualitatively similar, but quantitative results are different. We started by comparing the two-dimensional version of our model with their work. Anderson & Davis (1995) studied the contact angle as a function of time and found it to be almost constant over a significant period of time, followed by a sharp drop in the value at the final stages of evaporation. Our results indicate a more gradual change of the contact angle. We argue that this difference is due to taking into account nonlinear coupling between various contributions to the contact angle as opposed to a linear superposition of them. Next, we carried out derivation and numerical solution for the axisymmetric case and compared it with the two-dimensional treatments. The droplet turns out to evolve faster for the axisymmetric case. The axisymmetric version of our model is compared with recent experimental data on evaporating droplets of butanol.

Finally, we note that no instabilities are discussed in this paper. However, our approach provides a natural and physically based framework for both analytical and numerical studies of a variety of contact-line instabilities. Evolution of droplets of arbitrary shapes in three-dimensional configurations can be easily treated numerically by imposing the condition of constant adsorbed film thickness on the boundary of a computational domain of a simple, e.g. circular or rectangular, shape. The difficulty of describing the moving contact line will then be eliminated.

REFERENCES

Ajaev, V. S. & Homsy, G. M. 2001 Steady vapour bubbles in rectangular microchannels. *J. Colloid Interface Sci.* **240**, 259–271.

Anderson, D. M. & Davis, S. H. 1995 The spreading of volatile liquid droplets on heated surfaces. *Phys. Fluids* **7**, 248–265.

Bascom, W. D., Cottington, R. L. & Singleterry, C. R. 1964 Dynamic surface phenomena in the spontaneous spreading of oils on solids. In: *Contact Angle, Wettability, and Adhesion* (ed. F. M. Fowkes), pp. 355–379. ACS, Washington, DC.

Bourgés-Monnier, C. & Shanahan, M. E. R. 1995 Influence of evaporation on contact angle. *Langmuir* **11**, 2820–2829.

Braun, R. J., Murray, B. T., Boettinger, W. J. & McFadden, G. B. 1995 Lubrication theory for reactive spreading of a thin drop. *Phys. Fluids* **7**, 1797–1810.

Brown, P. N., Byrne, G. D. & Hindmarsh, A. C. 1989 VODE: a variable coefficient ODE solver. *SIAM J. Sci. Stat. Comput.* **10**, 1038–1051.

Burelbach, J. P., Bankoff, S. G. & Davis, S. H. 1988 Nonlinear stability of evaporating/condensing liquid films. *J. Fluid Mech.* **195**, 463–494.

Churaev, N. V., Starov, V. M. & Derjaguin, B. V. 1982 The shape of the transition zone between a thin film and bulk liquid and the line tension. *J. Colloid Interface Sci.* **89**, 16–24.

DasGupta, S., Schonberg, J. A., Kim, I. Y. & Wayner, P. C. 1993 Use of the augmented Young–Laplace equation to model equilibrium and evaporating extended menisci. *J. Colloid Interface Sci.* **157**, 332–342.

Dussan, V. E. B. 1979 On the spreading of liquids on solid surfaces: static and dynamic contact lines. *Annu. Rev. Fluid Mech.* **11**, 371–400.

Eggers, J. & Stone, H. A. 2004 Characteristic lengths at moving contact lines for a perfectly wetting fluid: the influence of speed on the dynamic contact angle. *J. Fluid Mech.* **505**, 309–321.

Ehrhard, P. & Davis, S. H. 1991 Non-isothermal spreading of liquid drops on horizontal plates. *J. Fluid Mech.* **229**, 365–388.

Ehrhard, P. 1993 Experiments on isothermal and non-isothermal spreading. *J. Fluid Mech.* **257**, 463–483.

de Gennes, P. G. 1985 Wetting: statics and dynamics. *Rev. Mod. Phys.* **57**, 827–863.

Glasner, K. B. 2003 Spreading of droplets under the influence of intermolecular forces. *Phys. Fluids* **15**, 1837–1842.

Glasner, K. B. & Witelski, T. P. 2003 Coarsening dynamics of dewetting films. *Phys. Rev. E* **67**, 016302.

Gokhale, S. J., Plawsky, J. L. & Wayner, P. C. 2003 Experimental investigation of contact angle, curvature, and contact line motion in dropwise condensation and evaporation. *J. Colloid Interface Sci.* **259**, 354–366.

Gramlich, C. M., Kalliadasis, S., Homsy, G. M. & Messer, C. 2002 Optimal leveling of flow over one-dimensional topography by Marangoni stresses. *Phys. Fluids* **14**, 1841–1850.

Greenspan, H. P. 1978 On the motion of a small viscous droplet that wets a surface. *J. Fluid Mech.* **84**, 125–143.

Haley, P. J. & Miksis, M. J. 1991 The effect of the contact line on droplet spreading. *J. Fluid Mech.* **223**, 57–81.

Hocking, L. M. 1993 The influence of intermolecular forces on thin liquid layers. *Phys. Fluids* A **5**, 793–799.

Hocking, L. M. 1995 On contact angles in evaporating liquids. *Phys. Fluids* **7**, 2950–2955.

Kabov, O. A. 2000 Breakdown of a liquid film flowing over the surface with a local heat source. *Thermophys. Aeromech.* **7**, 513–520.

Kandlikar, S. G. 2002 Fundamental issues related to flow boiling in minichannels and microchannels. *Exp. Therm. Fluid Sci.* **26**, 389–407.

Lopez, J., Miller, C. A. & Ruckenstein, E. 1976 Spreading kinetics of liquid drops on solids. *J. Colloid Interface Sci.* **56**, 460.

Miller, C. A. & Ruckenstein, E. 1974 The origin of flow during wetting of solids. *J. Colloid Interface Sci.* **48**, 368–373.

Moosman, S. & Homsy, G. M. 1980 Evaporating menisci of wetting fluids. *J. Colloid Interface Sci.* **73**, 212–223.

Morris, S. J. S. 2001 Contact angles for evaporating liquids predicted and compared with existing experiments. *J. Fluid Mech.* **432**, 1–30.

Oguz, H. N., Yuan, H. & Prosperetti, A. 1999 Growth and collapse of a vapour bubble in a small tube. *Intl J. Heat Mass Transfer* **42**, 3643–3657.

Potash, M. & Wayner, P. C. 1972 Evaporation from a two-dimensional extended meniscus. *Intl J. Heat Mass Transfer* **15**, 1851–1863.

Rose, J. W. 2000 Accurate approximate equations for intensive sub-sonic evaporation. *Intl J. Heat Mass Transfer* **43**, 3869–3875.

Wong, H., Morris, S. & Radke, C. J. 1992 Three-dimensional menisci in polygonal capillaries. *J. Colloid Interface Sci.* **148**, 317–336.

Wu, Q. & Wong, H. 2004 A slope-dependent disjoining pressure for non-zero contact angles. *J. Fluid Mech.* **506**, 157–185.

Zhornitskaya, L. & Bertozzi, A. 2000 Positivity-preserving schemes for lubrication-type equations. *SIAM J. Numer. Anal.* **37**, 523–555.